

A TIME DELAY MODEL FOR SOLAR AND STELLAR DYNAMOS

A. L. WILMOT-SMITH

School of Mathematics and Statistics, University of St. Andrews, North Haugh, St. Andrews, Fife, KY16 9SS, UK

D. NANDY

Department of Physics, Montana State University, Bozeman, MT 59717

G. HORNIG

Division of Mathematics, University of Dundee, 23 Perth Road, Dundee, DD1 4HN, UK

AND

P. C. H. MARTENS

Department of Physics, Montana State University, Bozeman, MT 59717

Received 2006 May 12; accepted 2006 July 27

ABSTRACT

Magnetohydrodynamic dynamos operating in stellar interiors produce the diverse range of magnetic activity observed in solar-like stars. Sophisticated dynamo models including realistic physics of convection zone flows and flux tube dynamics have been built for the Sun, for which appropriate observations exist to constrain such models. Nevertheless, significant differences exist in the physics that the models invoke, the most important being the nature and location of the dynamo α -effect and whether it is spatially segregated from the location of the Ω -effect. Spatial segregation of these source layers necessitates a physical mechanism for communication between them, involving unavoidable time delays. We construct a physically motivated reduced dynamo model in which, through the use of time delays, we mimic the generation of field components in spatially segregated layers and the communication between them. The model can be adapted to examine the underlying structures of more complicated and spatially extended numerical dynamo models with diverse α -effect mechanisms. A variety of dynamic behaviors arise as a direct consequence of the introduction of time delays in the system. Various parameter regimes give rise to periodic and aperiodic oscillations. Amplitude modulation leads to episodes of reduced activity, such as that observed during the Maunder minima, the length and duration of which depend on the dynamo number. Regular activity is more easily excited in the flux transport-dominated regime (when the time delay is smaller than the dissipative timescale), whereas irregular activity characterizes solutions in the diffusion-dominated regime (when the time delay is larger than the dissipative timescale).

Subject headings: stars: activity — stars: late-type — stars: rotation — Sun: activity — Sun: rotation

1. INTRODUCTION

Our understanding of the magnetohydrodynamic (MHD) dynamo mechanism, which is widely accepted to be the cause of stellar magnetism, relies mostly on observations of magnetic activity in our nearest star: the Sun. The solar cycle is manifested in a periodic variation in the number of sunspots and in the large-scale surface field evolution. The solar magnetic activity cycle, with an average period of 22 yr, has neither a regular length nor a regular amplitude. Half-cycle lengths, since detailed sunspot number records began in the early 17th century, have ranged from 7 to 14 yr (Ossendrijver 2003), with a steeper rising phase than declining phase. Cycle amplitudes have varied considerably both over the 400 yr sunspot observation span and on longer timescales. Activity records dating back several millennia can be reconstructed using cosmogenic isotopes as a proxy for solar activity (Beer et al. 1990) and show frequent reductions in cycle amplitude, the last of which is the Maunder minimum from AD 1645 to 1715 (e.g., Eddy 1988). However, there is evidence to suggest that the underlying magnetic cycle persists throughout grand minima (Beer et al. 1998), in spite of very few sunspot observations during the last observed one (Maunder minimum).

Although outside of phases such as grand minima the solar cycle can be characterized as approximately regular with minor variations in cycle amplitude and length, a relatively regular

cycle is not necessarily the only observed characteristic of a stellar MHD dynamo. A diverse range of activity is indicated in other solar-like stars. Using Ca II H and K emission as a proxy indicator, the global magnetic field of over 400 late-type stars has been recorded by the long-term Mount Wilson HK project (Baliunas et al. 1995). Results show a wide variety of activity (Baliunas et al. 1998), with around 60% of the sample showing cyclic variation, similar to the Sun. Of the remaining stars, a group show very variable emission in time with no clear periodicity, and the remainder show nearly constant emission. The possibility arises that some of the stars in this last category are in a Maunder minimum-type state. It turns out that the groups of stars with regular and irregular activity may be distinguished by their Rossby number (Ro)—the ratio of the star's rotation period to the convective turn over time. Irregular and strong emission are displayed by stars with $Ro < 1$, with regular activity, both cyclic and flat, displayed by those stars with $Ro > 1$ (Noyes et al. 1984a; Hempelmann et al. 1996; for a discussion, see Nandy 2004a).

It is highly likely that the nature of the dynamo, for any given star such as the Sun, has evolved over the lifetime of the star with the evolution of the properties of its convection zone, primarily mediated through spin-down and angular momentum losses via stellar winds. In this context, a brief consideration of some of the important parameters that determine the behavior of stellar dynamos might be useful (for more detailed discussions, interested

readers are referred to Noyes et al. 1984b and Montesinos et al. 2001). A measure of the efficiency of the dynamo mechanism is the dynamo number (N_D)—the ratio of the source terms to the dissipative terms in the dynamo equations—which depends on various physical properties of the stellar convection zone. Another important parameter that essentially describes the evolutionary state of stellar convection zones is the Rossby number, Ro . It can be shown that $N_D \sim 1/Ro^2$ (see, e.g., Durney & Latour 1978). Since the rotation period, depth of stellar convection zones, and convective turnover time evolve with stellar evolution, both N_D and Ro are expected to change over any given star's lifetime. Specifically, as stars age, their Rossby number increases with the corresponding increase in rotation period. Also, a wide variety of stars with different rotation periods and convection zone properties will have a wide range of N_D and Ro values. Indeed, one might therefore expect that the nature and output of the dynamo changes from one star to another and over the lifetime of any given star. Consequently, observations of stellar magnetic activity in a varied sample of solar-like stars (at different main-sequence ages and with different rotation rates) can be used to gain insights on the dynamo mechanism and study its evolution. This consideration, in part, motivates our present study.

If we assume, based on first principles, that similar properties of solar-like stars would allow them to host dynamos with similar physical properties, an ideal dynamo model should be able to account for the diverse range of magnetic activity in solar-like stars (including their regularities and irregularities), as well as other systematic patterns, such as Hale's polarity law observed in the Sun and the spatiotemporal evolution of starspots and large-scale stellar fields. While such a perfect and ideal model is the holy grail of stellar dynamo theorists, often a more utilitarian approach has been to understand various distinct mechanisms of such a dynamo, using diverse approaches, and then to use the insights gained to build a more complete picture. We briefly outline below the main characteristics of stellar dynamos that have been obtained through such studies (for detailed reviews, interested readers are referred to Ossendrijver 2003, Nandy 2003, and Charbonneau 2005).

The global stellar magnetic field may be decomposed into its constituent toroidal (in the direction of rotation) and poloidal (in the meridional plane) components. A mechanism for the generation of toroidal field from the poloidal component (known as the Ω -effect; Parker 1955) and for the subsequent regeneration of poloidal field from the toroidal component (the α -effect; Parker 1955) must exist. Solar observations (for example, the tracking of surface features such as sunspots) indicate a differential rotation, with the equator rotating faster than the poles. Helioseismology has shown that this persists throughout the convection zone (Schou et al. 1998), with the rotation varying mostly latitudinally. In a thin layer between the convection zone and the radiative layer, known as the tachocline, a strong radial shear in the angular velocity exists.

This differential rotation draws out the frozen-in poloidal field to form toroidal field through the Ω -effect. It also acts to amplify the toroidal field, and if the Ω -effect occurs largely in the tachocline layer, then flux storage (due to the subadiabatic temperature gradient and the consequent suppression of buoyancy there) can occur over timescales that are sufficiently long for strong fields to be built. Evidence of surface differential rotation has been found in other stars, and it is very likely that these persist to greater depths, as in the Sun. Thus, the Ω -effect is possibly a common mechanism for toroidal field generation in stars.

Several mechanisms have been proposed for the regeneration of the poloidal field from the toroidal component. Examples in-

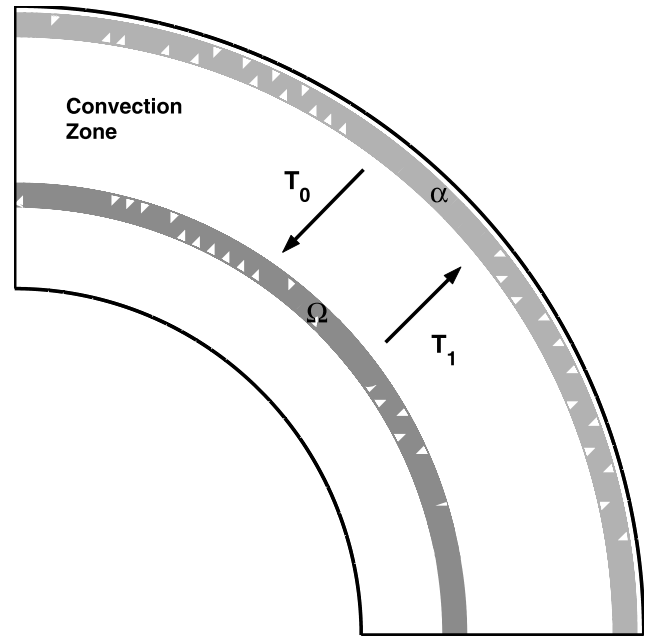


FIG. 1.—Cartoon depicting the concept of flux transport time delays in the interior of a solar-like star. This meridional cut (in the r - θ plane) shows the convection zone and some of the radiative interior. A region of strong shear in the differential rotation (such as the solar tachocline) is depicted in dark gray; the dynamo Ω -effect (which generates toroidal field from the poloidal component) acts in this layer. The dynamo α -effect (which regenerates poloidal field from the toroidal component) is shown here in light gray and acts in a layer located near the surface; the location of the α -effect layer depends on which physical mechanism is invoked to account for it (see text). For the dynamo to function, communication between the two segregated dynamo source layers should take place via some means of flux transport. This process involves unavoidable time delays. In this paper, the time taken for poloidal flux to be transported from the α -effect layer to the Ω -effect layer and toroidal flux to be transported from the Ω -effect layer to the α -effect layer are quantified in the time delays T_0 and T_1 , respectively.

clude a convective α -effect throughout the convection zone based on the twisting of toroidal fields by helical turbulence (Parker 1955; Tobias 1997), an α -effect in or near the tachocline arising from instabilities in the plasma flows or buoyantly rising magnetic flux tubes (Dikpati & Gilman 2001; Ferriz-Mas et al. 1994), and the decay of tilted bipolar sunspot pairs near the solar surface, known as the Babcock-Leighton mechanism (Babcock 1961; Leighton 1969; Durney 1997; Dikpati & Charbonneau 1999; Nandy & Choudhuri 2002; Chatterjee et al. 2004).

Which of these various proposed α -effect mechanism(s) is (are) dominantly at work in stellar interiors such as the solar convection zone is a matter of debate. What is certain is that these different α -effect mechanisms work at different layers in the convection zone and may or may not spatially coincide with the Ω -effect. The latter, for the Sun, is believed to be primarily in the tachocline layer. For the dynamo to work with a spatial segregation of the two source layers for the Ω - and α -effects, there has to be an efficient means of communication (through flux transport) between the two distinct source regions (see Fig. 1 for a discussion of the spatial geometry of the problem). Magnetic buoyancy plays a partial role in this by transporting strong toroidal flux from the base of the convection zone to the upper layers (i.e., from the Ω -effect layer to the α -effect layer). How the dynamo loop is closed through flux transport from the α -effect layer back to the Ω -effect layer differs from one model to another, based on which α -effect mechanism the model invokes.

For an α -effect operating in the tachocline, which is also the location of the Ω -effect, the spatial coincidence implies that the

communication between the source layers is almost instantaneous; that is, that the toroidal field generated by the Ω -effect is immediately available for regenerating the poloidal field. In the interface dynamo (Parker 1993), based on the convective α -effect, a negative convective α -effect is located in the convection zone only, below which the Ω -effect operates in the tachocline. A discontinuity in the magnetic diffusivity occurs across the interface between the tachocline and the convection zone. The separation of sites for the generation of poloidal and toroidal fields means that they interact primarily through diffusion or turbulent flux pumping (Tobias et al. 2001), which is the primary transporter of flux from the α -effect layer in the convection zone back to the Ω -effect in the tachocline. The same spatial physical structure characterizes dynamos based on an α -effect due to buoyancy instabilities and located just above the tachocline or in the base of the convection zone (Ferriz-Mas et al. 1994). A larger segregation of the two source layers differentiates the spatial physical structure of the Babcock-Leighton mechanism, where a positive α -effect acts in the surface layers. In this case it is advective flux transport by meridional circulation (see Nandy 2004b for a review), and to some extent turbulent pumping, that transports the surface poloidal flux to the tachocline where the Ω -effect resides. An unavoidable time delay due to the finite time required to transport magnetic flux from one source region to another materializes in those dynamo models that have physically distinct source layers. In this paper, we aim to explore the role of this time delay in solar and stellar dynamo activity.

It is important to realize that stellar magnetic activity observations present a wide range of parameter space to validate any stellar dynamo model. However, building sophisticated numerical dynamo models to explain the full range of dynamic behavior displayed by stars is a formidable task, more so in the absence of observed constraints on large-scale plasma flows in their interior. One approach to stellar dynamo modeling has been to use simplified models in which a qualitative comparison to solar observations is taken; several low-dimensional systems of ordinary differential equations (ODEs) have been proposed as illustrative dynamo models. Their dynamics are studied both to aid investigation of the full partial differential equation (PDE) models and to increase understanding of the dynamics that may be associated with nonlinear interactions. Such models may be derived using normal form theory of dynamical systems (Tobias et al. 1995; Wilmot-Smith et al. 2005) or by truncating at various orders a suitable form of the mean-field dynamo equations (Roald & Thomas 1997; Schmalz & Stix 1991; Weiss et al. 1984). A wide variety of dynamical behaviors occur in these low-dimensional models, including various types of intermittency that may account for events such as grand minima (Covas & Tavakol 1997). However, the removal of all spatial dependence in low-order models' descriptions of the field evolution gives an implied instantaneous communication between the two field components (toroidal and poloidal) that would not occur in spatially segregated models. The introduction of certain time delays in a system of ODEs, thus converting them to a set of delay differential equations (DDEs), can take account of such a spatial segregation. Indeed, time delays are intrinsic to PDE models that include meridional circulation, since this circulation effectively introduces a delay that is comparable to the cycle period.

The notion of time delay has been studied in the context of a finite delay in the feedback of the magnetic fields on the dynamo source terms (Yoshimura 1978). Time delay dynamics have also been examined in the specific case of the Babcock-Leighton model via the use of one-dimensional (1D) iterative maps (Durney 2000; Charbonneau 2001) that include the long time delay between

the production of toroidal field from poloidal field, but ignore dissipative effects. Results have been shown to be in good agreement with spatially extended numerical models (Charbonneau et al. 2005). Thus, in addition to stochastic forcing and dynamical nonlinearity, the possibility arises that observed irregularities in solar and stellar cycles may result from the effect of time delays in the underlying physical process that generates these cycles.

Here we introduce time delays into a set of truncated dynamo equations, thus constructing a time-delayed system that includes both dissipative effects (which are absent in 1D iterative maps) and a delay in both the conversion processes (from toroidal to poloidal component and vice versa). The underlying physical mechanism remains relatively transparent and can, in general, be applied to study dynamo models based on a diverse set of α -effect mechanisms. In this model, a low or vanishing time delay physically resembles a scenario in which the dynamo α -effect and Ω -effect are spatially coincident. Finite time delays properly account for the two-layer character of dynamos based on spatially segregated source regions and the role that magnetic flux transport (e.g., mediated via meridional circulation or magnetic buoyancy) plays in these models. It is shown that the introduction of time delays can have a considerable effect on the dynamics and can lead to significant fluctuations in cycle amplitude.

In § 2 we derive the model, before examining its behavior in two important parameter regimes in § 3. One regime is that for which the time delay is smaller than the dissipative timescale. We characterize solutions in this regime, where the effect of the time delays dominates over that of dissipation, as *flux transport-dominated*, and find that relatively regular activity identifies these solutions. The case where the time delay is larger than the dissipative timescale is characterized as the *diffusion-dominated* regime, and we find that irregular activity is more easily excited in this case. We discuss the implications of our results for solar and stellar dynamos and conclude in §§ 4 and 5.

2. MODEL SETUP

Considering only the source and dissipative processes in the dynamo mechanism and through a truncation via removal of all spatial dependence, we obtain the equations

$$\begin{aligned}\frac{dB_\phi}{dt} &= \frac{\omega}{L}A - \frac{B_\phi}{\tau}, \\ \frac{dA}{dt} &= \alpha B_\phi - \frac{A}{\tau},\end{aligned}$$

where B_ϕ represents the toroidal field and A represents the poloidal field. In this simplest possible case, the evolution of each component is a result of the combination of a source process (first term on the right-hand side of the above equations) and a diffusive process (second term on the right-hand side). For the toroidal field, the source process is a conversion from the poloidal field (the Ω -effect), dependent on the differential rotation ω (not to be confused with the rotation rate) and the length scale over which it acts, L (the length of the tachocline, for example). Diffusion of the field itself, occurring through ohmic decay, is parameterized by τ , which represents the diffusion timescale for the magnetic field. The evolution of the poloidal field is also a combination of two similar actions: diffusion, again governed by τ , and a source in the conversion from toroidal field via the α -effect. Note, however, that there are no growing solutions to these equations and so no dynamo action can occur.

To account for α -quenching, we take a general form for α given by $\alpha = \alpha_0 f$, where α_0 is the amplitude of the α -effect

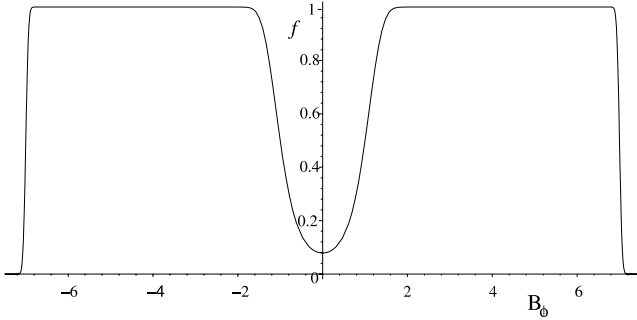


FIG. 2.—Dependence of the quenching factor, f (given by eq. [1]), on toroidal field strength, for the parameters $B_{\min} = 1$ and $B_{\max} = 7$.

and f is the quenching factor, approximated here by the nonlinear function

$$f = \frac{[1 + \operatorname{erf}(B_\phi^2(t) - B_{\min}^2)][1 - \operatorname{erf}(B_\phi^2(t) - B_{\max}^2)]}{4}. \quad (1)$$

Figure 2 illustrates a typical profile for f . Thus, B_{\max} is the upper limit to the toroidal field strength on which the α -effect can act, and B_{\min} is the lower limit (which can be set to zero). The lower limit B_{\min} comes from a critical threshold in the toroidal field in stellar interiors above which toroidal flux ropes become magnetically buoyant and rise up into the α -effect source region for poloidal field generation to take place. This lower threshold due to magnetic buoyancy is known to limit field strengths and has been shown to play a crucial role in determining the amplitude of dynamo activity (Nandy 2002). The upper limit B_{\max} is associated with α -quenching in mean-field dynamo models (via the Lorentz feedback of strong toroidal fields on helical turbulence), while in the Babcock-Leighton mechanism the limit results from the ineffectiveness of the Coriolis force on strong toroidal flux tubes, which therefore rise with no significant tilt (D’Silva & Choudhuri 1993; Fan et al. 1994).

In a dynamo with spatially segregated source regions, communication between the two layers would not be instantaneous, as is assumed in the above equations. To take account of this, two physically motivated distinct time delays are introduced into the equations, the first being a time delay for the conversion of poloidal field into toroidal field, T_0 , and the second a time delay for the conversion of toroidal field into poloidal field, T_1 (see Fig. 1). Time delays will appear in all conversion processes, and so the equations become

$$\frac{dB_\phi(t)}{dt} = \frac{\omega}{L} A(t - T_0) - \frac{B_\phi(t)}{\tau}, \quad (2)$$

$$\frac{dA(t)}{dt} = \alpha_0 f(B_\phi(t - T_1)) B_\phi(t - T_1) - \frac{A(t)}{\tau}. \quad (3)$$

Thus, a system of two coupled DDEs has been obtained to describe the dynamo, with the only nonlinearity being the parameterization of the source term for the poloidal field. The time delays signify that the generation of any component of the magnetic field (on the left-hand side of the above equations), at a given instant in time, is dependent on the magnitude of the other component of the magnetic field (appearing in the first term on the right-hand side) at an earlier time, corresponding to the time delay. Thus, this system of DDEs has an built-in memory mechanism capable of “remembering” the values of magnetic fields from

an earlier time equal to the time delays. We show in § 3 that growing solutions to these equations are possible.

The time delay T_0 accounts for the time taken for a poloidal flux tube to be transported from the site of its production back to the tachocline. In the Babcock-Leighton mechanism the meridional circulation advects surface poloidal field back to the tachocline (which, from midlatitudes at the surface to midlatitudes at the tachocline, takes on the order of 10 yr). Often invoked in the high magnetic Reynolds number (Re_m) regime, this class of advection-dominated models assumes that there are negligible dissipative losses during this transport. The meridional circulation then governs T_0 in Babcock-Leighton models. We might expect the delay to be shorter in the interface dynamo (with downward flux transport accomplished by turbulent flux pumping, which again has negligible dissipative effects during transport), particularly if the α -effect is deep-seated. The time delay should be vanishingly small for spatially coincident source layers (with both the Ω - and α -effects in the tachocline, for example). Note that to some extent, poloidal flux can be brought down to the Ω -effect layer through simple spatial diffusion (as opposed to other mechanisms, this also destroys the flux during transport). If indeed the spatial diffusive transport is faster and more efficient than all other means of transport, then T_0 should correspond to the spatial diffusion timescale, and one has to account for dissipation during flux transport (see § 4 for a discussion on this). The important point to remember is that if there are competing mechanisms for flux transport, the one with the shortest timescale should be the governing one (as this would be most efficient).

The time delay T_1 accounts for the time taken for a toroidal flux tube to buoyantly rise to the site of poloidal field production. The timescale for the buoyant rise of a flux rope from the interior to the photosphere is rather short, being on the order of 3 months, and so $T_1 \ll T_0$. However, $T_{0,1} \neq 0$ in any model for which there is a spatial segregation between the two layers.

The diffusion timescale for the magnetic field is given by

$$\tau = \frac{L_{\text{SCZ}}^2}{\eta},$$

where L_{SCZ} is the width of the solar convection zone (in general, it should be the separation of the two source layers); $L_{\text{SCZ}} = 0.3 R_\odot \sim 2.1 \times 10^8$ m. A widely accepted value for the diffusivity is $\eta \sim 10^{12}$ cm² s⁻¹, and so $\tau \sim 13.8$ yr.

Given the novel character of the model, we choose to explore a wide range of parameter space. The brief discussion of the parameter values above is intended primarily to provide an indication of the relative magnitudes of the terms, which is shown later to be critical in determining dynamics. However, we make no attempts here to reproduce actual solar or stellar values and instead focus on the qualitative behavior of the model in different parameter regimes. Therefore, for ease of exposition, we present all the results in dimensionless form. We may recover information about the magnetic field strengths and timescales obtained in the results by comparing the nondimensional quantities to reference values; for example, to B_{\max} and to τ . The parameter B_{\max} represents the upper limit to the toroidal field strength on which the α -effect can act, and τ represents the diffusive timescale for the magnetic field. The values $B_{\max} \approx 10^5$ G and $\tau \approx 13.8$ yr (as derived above) are suggested from flux tube dynamics simulations and solar observations, respectively, but may be different for other solar-type stars.

As an aid to understanding the underlying structure of the model, we can reduce the system of equations (2) and (3) to a single second-order equation for B_ϕ by differentiating equation (2)

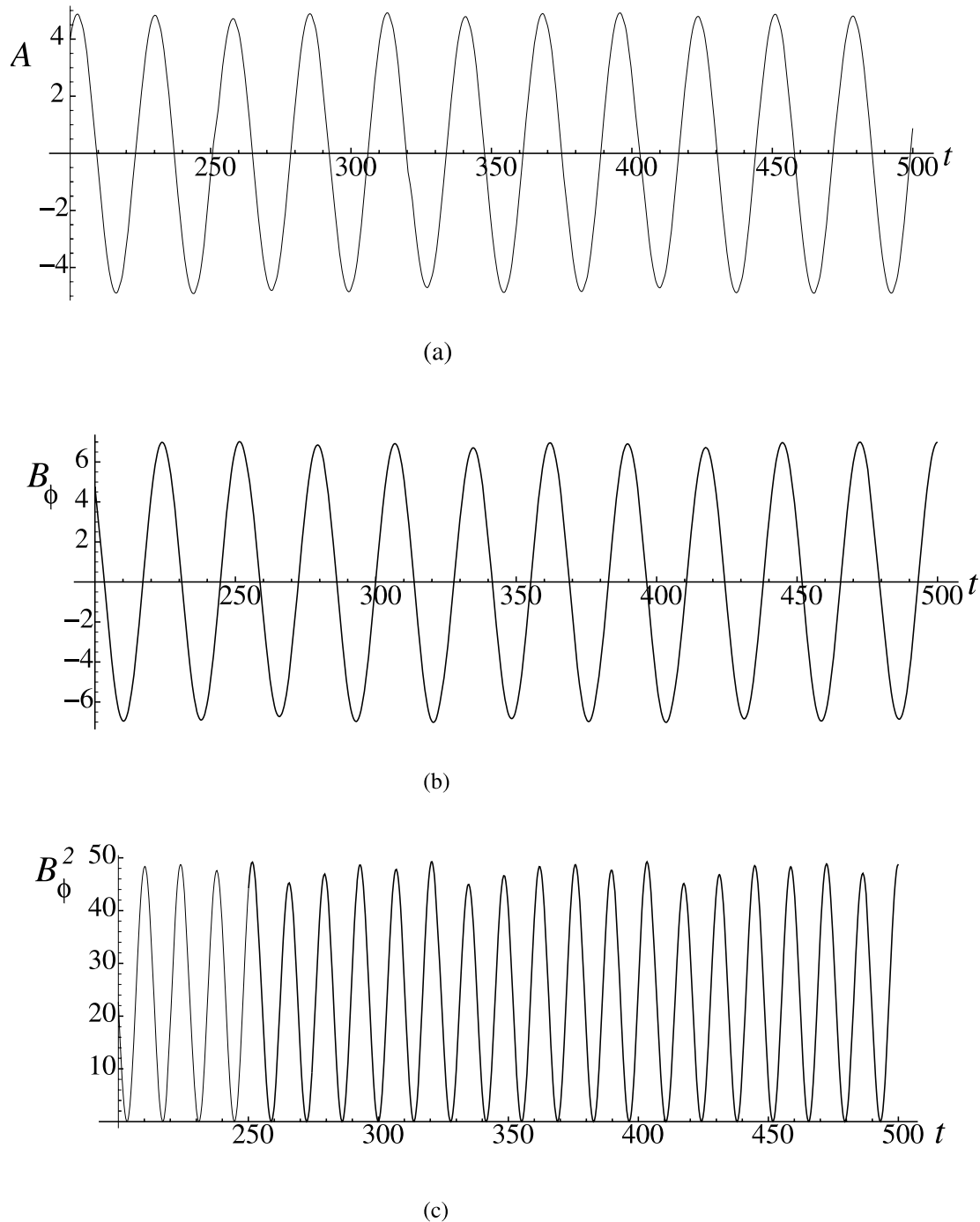


FIG. 3.—Time series, in the flux transport–dominated regime, for (a) the poloidal field, (b) the toroidal field, and (c) the magnetic activity (energy), B_ϕ^2 , for dynamo number $N_D = -13.01$ and the parameters $\tau = 15$, $B_{\min} = 1$, $B_{\max} = 7$, $T_0 = 2$, $T_1 = 0.5$, $\omega/L = -0.34$, and $\alpha_0 = 0.17$.

and substituting equation (3) for $dA(t - T_0)/dt$ [note the evaluation at the delayed time $(t - T_0)$]. The term proportional to $A(t - T_0)$ generated by this step in turn is substituted for by equation (2). The resulting equation is

$$\frac{d^2 B_\phi}{dt^2} + \frac{2}{\tau} \frac{dB_\phi}{dt} + \frac{1}{\tau^2} B_\phi = \frac{\alpha_0 \omega}{L} f(B_\phi(t - T_0 - T_1)) \times B_\phi(t - T_0 - T_1), \quad (4)$$

which can be supplemented by equation (2) for the solution of $A(t)$. The system of equations (2) and (4) is equivalent to the

system of equations (2) and (3) and therefore has the same set of solutions.

The time delays T_0 and T_1 appear in equation (4) as a sum, so it appears to be their sum that is important in determining the dynamics. If the right-hand side of equation (4) is set to zero, the equation becomes that of a critically damped oscillator. Thus, for toroidal field strengths outside of the range where f is nonzero, we might expect the system to behave as a critically damped oscillator. For toroidal field strengths within the range where f is nonzero, the term on the right-hand side of equation (4) is important. We will show in § 3 that some

analogies of the full system with a damped driven oscillator can be made.

To examine solutions to this system, we numerically integrate the equations, basing the code on the `NDelayDSolve.m` package in Mathematica. An initial solution to the problem in the range $t \in [-T_{\max}, 0]$ is specified, where $T_{\max} = \max\{T_0, T_1\}$. The effect of various initial conditions is discussed as the solutions are presented.

The model is relatively simple, but it gives rise to a wide range of dynamic behavior. Here some parameter regimes are examined that suffice to illustrate the complexity that the system is capable of displaying and its relevance to our understanding of solar and stellar dynamos. From equation (4), the sum of the two time delays is expected to be important in determining the dynamics. Therefore, we examine two extreme cases in particular. One case is where $\tau \gg T_0 + T_1$, which we call the flux transport-dominated regime and consider in § 3.1. The case in which $\tau \ll T_0 + T_1$ is called the diffusion-dominated regime and is considered in § 3.2. In both of these regimes we consider solutions for positive and negative dynamo number, N_D (which is related to the Rossby number as $N_D \propto 1/\text{Ro}^2$; Durney & Latour 1978). In particular we consider the effect of increasing $|N_D|$, since from stellar observations a change in the dynamics is expected across a parameter space covering a range of N_D (and consequently Ro) values.

3. RESULTS

Setting $T_0 = T_1 = 0$ in equations (2) and (3) corresponds to a dynamo model in which there is no time delay in the magnetic flux transport between the two source regions (a situation that could result when the source regions are spatially coincident and there is no time delay involved in the α -quenching mechanism via the Lorentz feedback). In this two-dimensional system, when the condition $\tau > 0$ is applied, we obtain only two qualitatively different solutions; either A and B_ϕ both decay to zero, or they are both attracted to a nonzero fixed point of the system. These fixed points are given by solutions $A(t) = a$, $B_\phi(t) = b$, such that $f(b) = L/(\alpha_0 \omega \tau^2)$ and $a = Lb/\omega \tau$. Thus, the solutions described in the following sections all arise from the inclusion of time delays in the model. A simple dynamo model in which the α -effect and the shear effect are concentrated in separate layers and communicate through diffusion was presented by Moffatt (1978, p. 216). An analytical analysis showed that dynamo action cannot occur within the model when the two layers are spatially coincident. We note also that in the linear analysis of the dynamo equations, Parker (1955) found wave-type solutions when the spatial derivatives are explicitly accounted for. The time delays we will introduce later compensate for the information lost by simplifying the spatial terms as we have above.

When at least one of the time delays is nonzero, oscillatory solutions to the system may be obtained. In the solar case, the strength of the toroidal field is much greater than that of the poloidal field. This can always be reproduced for nonzero solutions by taking $|\omega_0/L| > |\alpha_0|$. Although $\langle B_\phi \rangle > \langle A \rangle$ may also be achieved in some parameter regimes with $|\omega_0/L| < |\alpha_0|$, these cases are more limited. The parameters B_{\min} and B_{\max} are fixed throughout as $B_{\min} = 1$ and $B_{\max} = 7$. Qualitatively similar solutions to those outlined below can be attained with different particular values of B_{\min} and B_{\max} ; see § 4 for a further discussion of this point.

3.1. Flux Transport-dominated Regime

Solutions obtained in the regime where the diffusion timescale is large compared to the time delays ($\tau > T_0 + T_1$) are examined

in this section. Physically, this scenario means that the flux transport (mediated by any of, or the collective action of, meridional circulation, magnetic buoyancy, and turbulent flux pumping) occurs efficiently and within a duration of time over which dissipative effects are not important.

In this model the dynamo number is given by $N_D = \alpha_0 \omega \tau^2 / L$. We begin by examining solutions for $N_D < 0$, using $\omega < 0$ and $\alpha_0 > 0$, and taking a sequence of increasing absolute values of the dynamo number N_D (and therefore of decreasing Rossby number Ro). This corresponds to increasing the rotation rate of the star. The cut through parameter space given by $\omega/L + 2\alpha_0 = 0$ is taken, so that the relative strength of the source terms for poloidal and toroidal field production remain the same, and all other parameters are fixed as $\tau = 15$, $B_{\min} = 1$, $B_{\max} = 7$, $T_0 = 2$, $T_1 = 0.5$, and $\omega/L + 2\alpha_0 = 0$. The initial solutions are specified as the constant $(B_{\min} + B_{\max})/2$ for both A and B_ϕ .

On this sequence a periodic orbit bifurcates from the fixed point at the origin when $N_D = -12.696$. The orbit then becomes periodically modulated, so that B_ϕ and A both show oscillatory behavior, with amplitudes modulated on a longer timescale. The amplitude of modulation increases along the parameter path, but B_ϕ lies within the range $[-B_{\max}, B_{\max}]$ for all time. An example is shown in Figure 3, where $N_D = -13.01$.

For $N_D < -17.11$ solutions for B_ϕ are no longer contained within the range $[-B_{\max}, B_{\max}]$. Solutions are now periodic, with both A and B_ϕ showing cyclic behavior, with a constant period and amplitude, a typical example of which is illustrated in Figure 4. The rising phase of both solutions is steeper than the declining phase, and a sharp change in the first derivatives of both A and B_ϕ can be seen during each declining phase.

Both the period and amplitude of the oscillation increase with increasing $|N_D|$, as shown in Figure 5. There is a linear dependence of amplitude on dynamo number over several orders of magnitude, while the period of the cycle varies logarithmically.

As is evident from Figure 6, an increase in the sum $T_0 + T_1$ also increases both the periods and amplitudes. Solutions remain qualitatively the same as those illustrated in Figure 3 until $T_0 + T_1 \sim 50$.

Next we consider solutions for positive dynamo number, $N_D > 0$. Again, periodic solutions to the system can be obtained; however, there are important distinctions to be made from the case $N_D < 0$. On increasing the dynamo number, the first bifurcation leads to periodic solutions in which both $A(t)$ and $B_\phi(t)$ are of single sign only, and $B_\phi(t)$ is not contained within the range $[-B_{\max}, B_{\max}]$. A typical example is illustrated in Figure 7. The characteristic steep rising phase of the cycle and slower declining phase remain, as does the sharp change in the derivatives of A and B_ϕ at the end of each declining phase. The same qualitative dependence of cycle amplitude and period on both total time delay and $|N_D|$ as that for $N_D < 0$ is recovered.

Some analogies of solutions in this regime to a damped driven oscillator can be made to help explain these properties. Recall that a driven oscillator with periodic driving force can be described by the equation

$$\frac{d^2x}{dt^2} + \frac{b}{m} \frac{dx}{dt} + \frac{k}{m} x = -\beta \cos(\Omega t)$$

(where $\beta > 0$), which has the steady state solution

$$x(t) = \frac{\beta}{\sqrt{b^2 \Omega^2 / m^2 + [(k/m) - \Omega^2]^2}} \cos(\Omega t + \Phi),$$

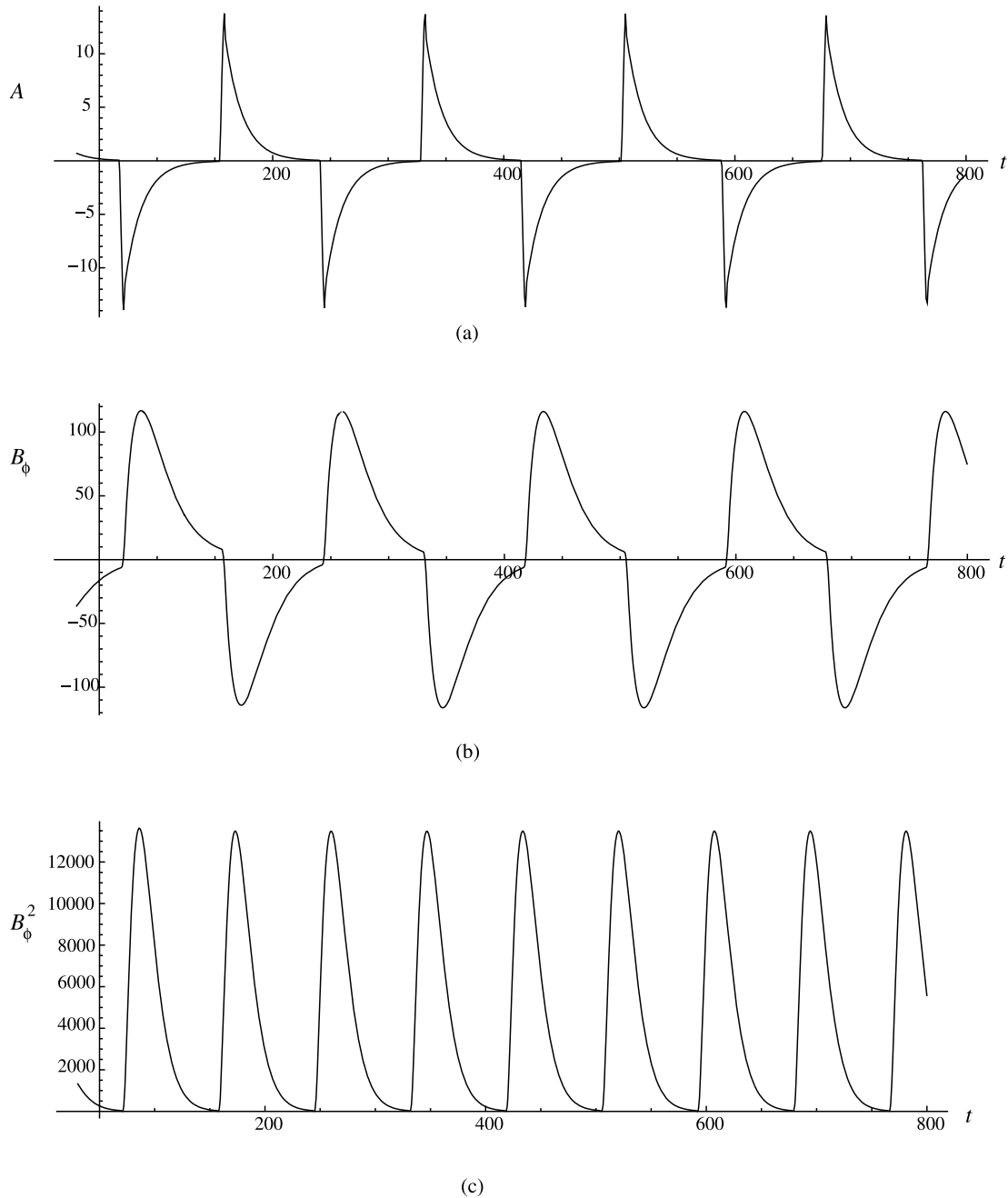


FIG. 4.—Typical time series for $N_D < 0$ in the flux transport–dominated regime for (a) the poloidal field, (b) the toroidal field, and (c) the magnetic activity. Here the parameters $\omega/L = -1.5$, $\alpha_0 = 0.75$, $B_{\min} = 1$, $B_{\max} = 7$, $\tau = 15$, $T_0 = 2$, and $T_1 = 0.5$ have been used.

where Φ represents the phase shift and is given by

$$\Phi = \operatorname{arccot}\left(\frac{\Omega^2 m - k}{\Omega b}\right). \quad (5)$$

The nonzero time lags mean that the right-hand side of equation (4) is out of phase with the solution. Thus, this term acts as a driver to the system while $B_\phi(t - T_0 - T_1)$ is within the range $[-B_{\max}, B_{\max}]$, which we call the forcing region.

For negative dynamo number, along the sequence of increasing $|N_D|$, the first bifurcation results in a periodic solution contained entirely within the range $[-B_{\max}, B_{\max}]$. Thus, for this solution $f \sim 1$ and $B_\phi(t) = B_0 \cos(\Omega t)$. If $f = 1$ in equation (4), assum-

ing the driver acts purely sinusoidally as $B_0 \cos(\Omega(t - T_d))$, where $T_d = T_0 + T_1$, we find

$$B_\phi(t) = \frac{-N_D B_0}{1 + \Omega^2 \tau^2} \cos\left(\Omega(t - T_d) + \operatorname{arccot}\left(\frac{\Omega^2 \tau - (1/\tau)}{2\Omega}\right)\right).$$

This expression must be equivalent to our assumption, $B_\phi(t) = B_0 \cos(\Omega t)$, and so equating the two expressions gives

$$\Omega T_d = \operatorname{arccot}\left(\frac{\Omega^2 \tau - (1/\tau)}{2\Omega}\right), \quad (6)$$

$$\frac{-N_D}{1 + \Omega^2 \tau^2} = 1. \quad (7)$$

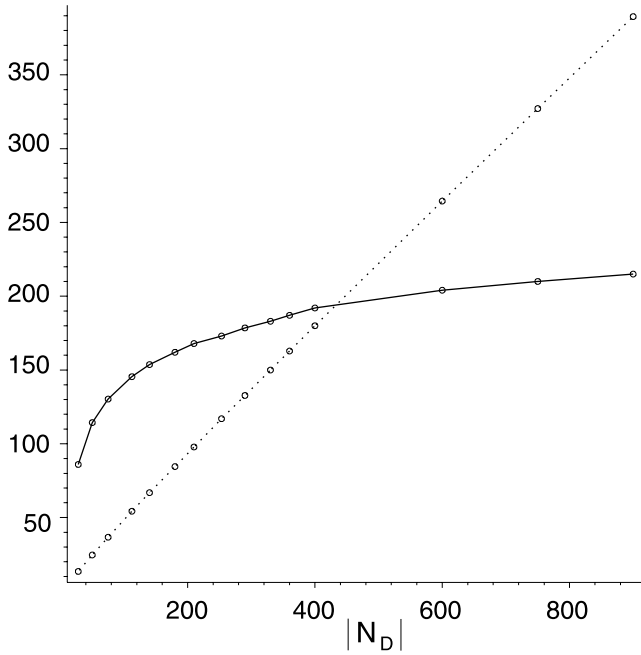


FIG. 5.—Change of cycle period (solid line) and amplitude (dotted line) with the magnitude of the dynamo number, $|N_D|$, in the flux transport-dominated regime for $N_D < 0$. The parameters are $\tau = 15$, $B_{\min} = 1$, $B_{\max} = 7$, $T_0 = 2$, $T_1 = 0.5$, and $\omega/L + 2\alpha_0 = 0$.

We may use this equivalence to explain the value at which the periodic orbit bifurcates from the fixed point and also the frequency of the resultant oscillation. For the parameter values used above, $T_d = 2.5$ and $\tau = 15$, equation (6) implies $\Omega = 0.228$, for which the corresponding oscillation period is $P = 27.58$. Given this value for Ω , N_D can be deduced from equation (7) as $N_D = -12.67$. These values correspond closely to the bifurcation value

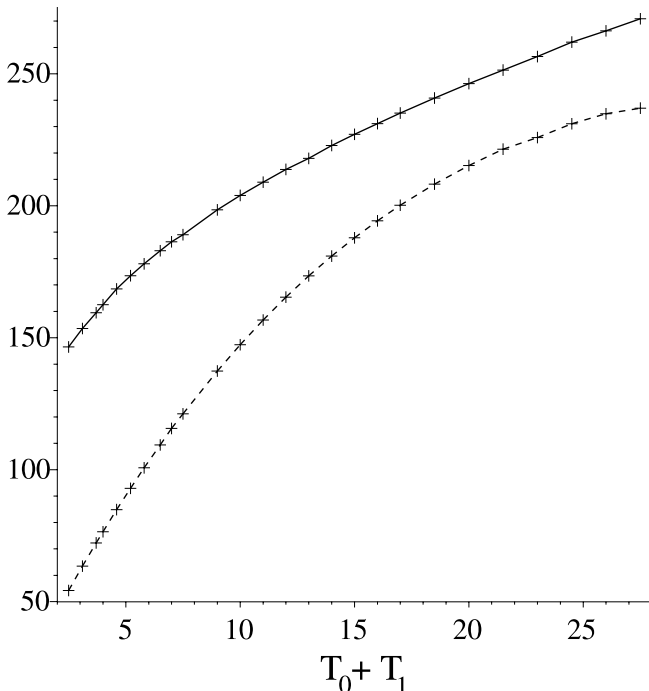


FIG. 6.—Change of cycle period (solid line) and amplitude (dashed line) with time delay $T_0 + T_1$ in the flux transport-dominated regime for $N_D < 0$. The parameters are $\tau = 15$, $B_{\min} = 1$, $B_{\max} = 7$, $\omega/L = -1$, $\alpha_0 = 0.5$, and $T_0 = 4T_1$.

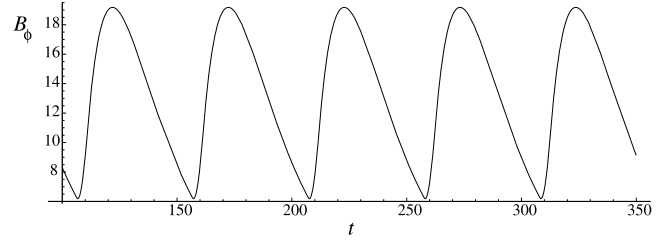


FIG. 7.—Typical time series for the toroidal field for $N_D > 0$ in the flux transport-dominated regime. The parameters $\omega/L = -0.5$, $\alpha_0 = -0.2$, $B_{\min} = 1$, $B_{\max} = 7$, $\tau = 15$, $T_0 = 2$, and $T_1 = 0.5$ have been used, and the initial solution is $B_\phi(t) = -5$ and $A(t) = -5$ over the range $t \in [-2.5, 0]$.

found in the simulations of $N_D = -12.696$, for which the simulated period was $P = 27.54$. Since $\cos(\Omega t + \Phi) = -\cos(\Omega t + \Phi + \pi/2)$, we might also expect to obtain periodic solutions contained within $[-B_{\max}, B_{\max}]$ for $N_D > 1$. Instead, growing solutions are found, and indeed, for $f = 1$, there exist solutions to equation (4) of the form $B_\phi(t) \sim \exp(\lambda t)$ with real $\lambda > 0$ precisely when $N_D > 1$. Such solutions give rise to behavior such as that observed in Figure 7.

When the dynamo number is sufficiently high that solutions are not contained within the range $[-B_{\max}, B_{\max}]$, the analogy with the driven oscillator may still be used, but now with the driver acting only intermittently on the solution. Qualitatively, the cycle may be described as follows. The driver starts acting on the system at a time $T_0 + T_1$ after the solution $B_\phi(t)$ enters the forcing region and continues to act until a time $T_0 + T_1$ after the solution $B_\phi(t)$ has left the forcing region. This corresponds to the steep rising phase of the cycle. After this time, the term on the right-hand side of equation (4) is zero, and it becomes that of a damped oscillator. After reaching a maximum in its absolute value, the solution then decays until $B_\phi(t - T_0 - T_1)$ again enters the forcing region, where a sudden change in the gradient of $B_\phi(t)$ occurs as the driver again starts to act on the system.

The sign of the term on the right-hand side of equation (4) determines the nature of the driving. If this term has negative sign when it acts on the system, then the solution will be driven in the $-B_\phi$ direction, whereas if the term has positive sign, then the solution will be driven in the $+B_\phi$ direction. The lengthy diffusive timescales when compared to the time delays ensure that $B_\phi(t - T_0 - T_1)$ is of the same sign as $B_\phi(t)$ when $B_\phi(t)$ decays to $\pm B_{\max}$. Thus, if $N_D < 0$, the solution is forced in the same direction as the decay, and a change in the sign of the solution occurs. If $N_D > 0$, then the solution is forced against the direction of decay, and the resulting solutions are of single sign only.

This mechanism predicts an increase in the amplitude of the cycle if, for example, the strength of the driving is increased, or if the driving term acts on the system for a greater length of time. An increase in dynamo number $|N_D|$ by keeping τ fixed and increasing both α_0 and ω/L has the effect of increasing the amplitude of the forcing, since the term on the right-hand side of equation (4) depends on the product $\alpha_0\omega/L$. Over several orders of magnitude, as shown in Figure 5, there is a linear relationship between the cycle amplitude and the product $\alpha_0\omega/L$. Using equation (4), we expect the decay to be governed by $\exp(-t/\tau)$. Thus, with greater amplitude it will take a longer time for the system to decay and reenter the forcing region. This timescale agrees closely with values found in the simulations and predicts a period increasing logarithmically with amplitude, as is seen in Figure 5. The length of time for which the driving term acts on the system will depend on the sum of the time delays, since the driving term acts on the system until a time $T_0 + T_1$ after the solution $B_\phi(t)$ has

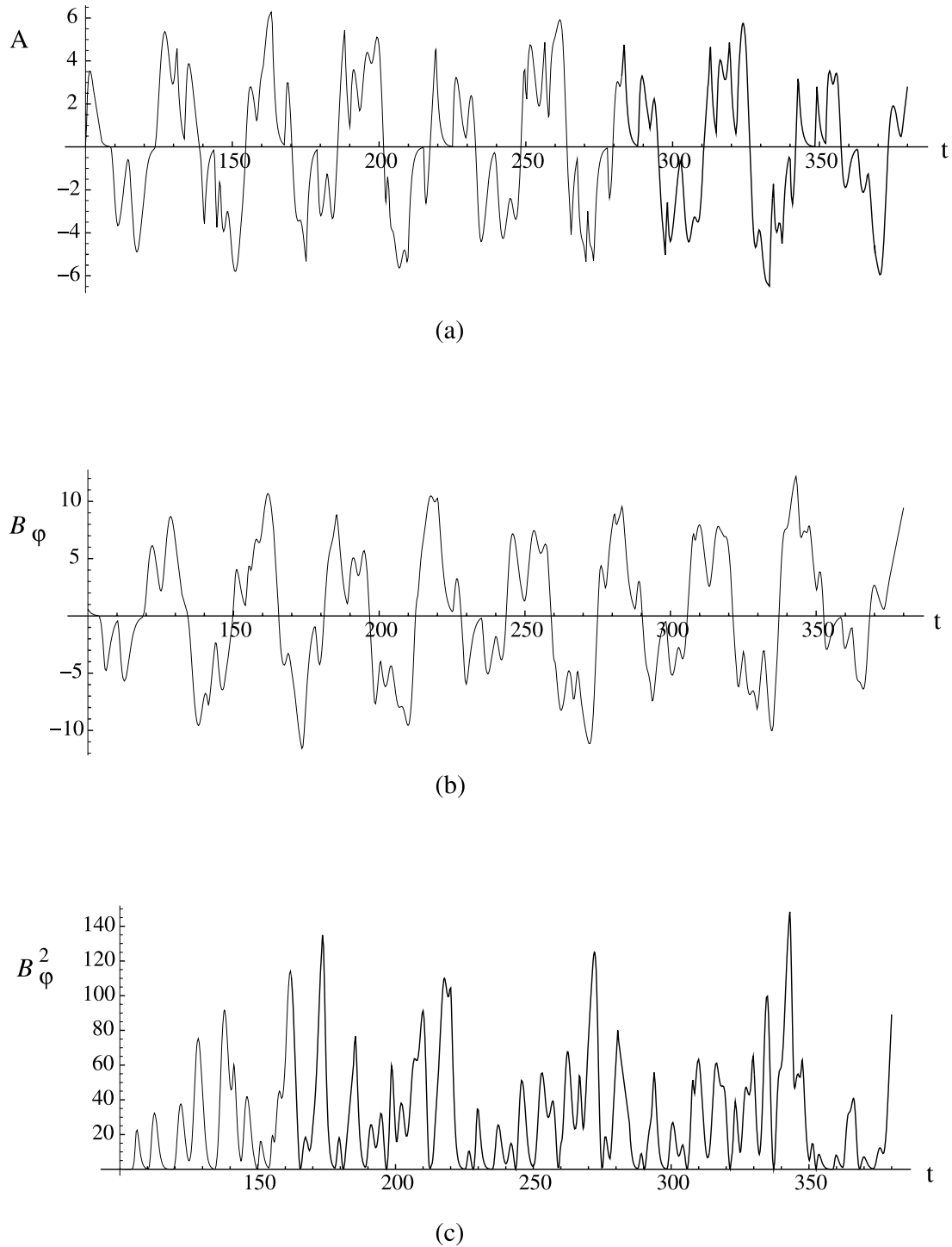


FIG. 8.—Diffusion-dominated regime time series with $N_D < 0$ for (a) the poloidal field, (b) the toroidal field, and (c) the magnetic activity, using the parameters $\omega/L = -2$, $\alpha_0 = 1$, $\tau = 1$, $T_0 = 10$, and $T_1 = 4$.

left the forcing region. Thus, an increase in the sum of the time delays also increases the amplitude of the oscillation, as shown in Figure 6, and accordingly the period of the oscillation.

It is worthwhile here to compare the behavior of this time-delayed system with numerical simulations of spatially extended solar dynamo models with realistic internal rotation profiles; specifically, those Babcock-Leighton models in which meridional circulation acts as a transporter of flux between the two source regions. If the circulation is fast (and so the time delay small),

the dynamo is more efficient and its period is smaller. Conversely, if the circulation is slow (and the time delay large), the period is higher (see Hathaway et al. 2003 for solar observations that support this argument and Nandy 2004b for a review on the role of meridional circulation in determining the period and amplitude of such dynamo models). Also, for slow circulation speeds (corresponding to large time delays in our model), although subject to the condition that the circulation timescale is still shorter than the diffusion timescale, since magnetic fields stay in the source

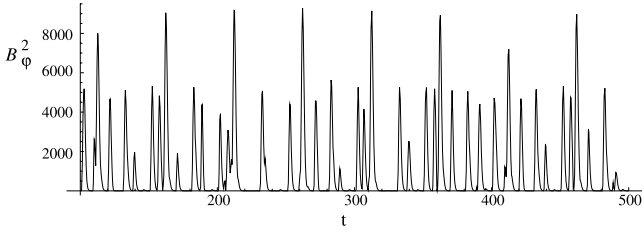


FIG. 9.—Time series for the magnetic activity with $N_D < 0$ and the parameters $\omega/L = -10$, $\alpha_0 = 5$, $\tau = 1$, $T_0 = 10$, and $T_1 = 4$.

regions for a longer time, the inductive effect results in higher amplitudes, in agreement with the results of our time-delayed system.

3.2. Diffusion-dominated Regime

Solutions for which the diffusion timescale is smaller than the time delays ($\tau \ll T_0 + T_1$) are discussed in this section. Physically, this corresponds to a scenario in which significant (ohmic) dissipation alters the magnitude of the fields on a timescale comparable to the flux transport between the source regions.

A wide variety of dynamics occur in this case. Again we begin by examining solutions for which $N_D < 0$. To illustrate some of these, we fix the parameters $\tau = 1$, $T_0 = 10$, and $T_1 = 4$ and examine a sequence of increasing absolute values of the dynamo number, N_D (with values of B_{\min} and B_{\max} unchanged). Again the cut through parameter space given by $\omega/L + 2\alpha_0 = 0$ is taken, so the relative strengths of the source terms for poloidal and toroidal field production remain the same. The initial solution is taken as the constant $(B_{\min} + B_{\max})/2$ for both A and B_ϕ .

For all initial conditions with $-1 < N_D < 0$, solutions are attracted to the fixed point at the origin, $A, B_\phi \rightarrow 0$. When $N_D < -1$, oscillatory solutions that are characteristically irregular are obtained. A typical example of solutions obtained at low dynamo number is illustrated in Figure 8, where the time series for the poloidal field, A , toroidal field, B_ϕ , and magnetic activity, B_ϕ^2 , are shown. Note that B_ϕ does not always lie within the range $[-B_{\max}, B_{\max}]$. Both A and B_ϕ show a long-term cycle (approximately 8.5 of which are illustrated here), where the fields oscillate between positive and negative signs and that is regular in its length, P . The parameters taken in Figure 8 result in an average period of $P = 31.6$ time units. Within each half-cycle the field also oscillates, leading to a time series for the magnetic activity that does not have an underlying magnetic sequence oscillating between positive and negative signs. Both the period and amplitude of the activity cycle are irregular.

As the dynamo number is increased, amplitude modulation leads to time spans where magnetic activity is considerably reduced, as is apparent in Figures 9 and 10. Although the basic cycle persists throughout these episodes, the field strengths are significantly below the average values. The episodes become more regular with increasing dynamo number; a pattern to the events

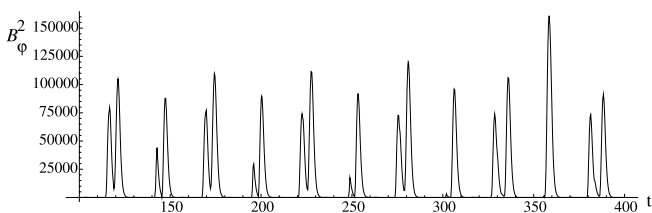


FIG. 10.—Time series for the magnetic activity with $N_D < 0$ and the parameters $\omega/L = -16$, $\alpha_0 = 8$, $\tau = 1$, $T_0 = 10$, and $T_1 = 4$.

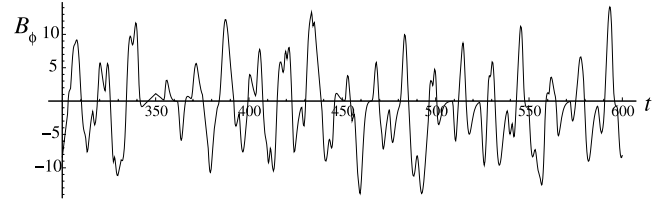


FIG. 11.—Time series for the toroidal field with $N_D > 0$ and initial solution $A(t) = B_\phi(t) = \cos(t)$. The parameters $\omega/L = -3$, $\alpha_0 = -1$, $\tau = 1$, $T_0 = 10$, and $T_1 = 4$ have been taken.

is clear in Figure 10, for example. Just as in the flux transport-dominated case, the amplitude of the oscillation increases with dynamo number, as illustrated in Figures 8–10. However, the maximum amplitude is now not constant from cycle to cycle. For a given set of parameters τ , T_0 , and T_1 , there exist certain parameter values ω/L and α_0 such that the amplitude of the solution is relatively regular, with Figure 10 providing an example of this. Fixing ω/L , α_0 , and τ in such a case and increasing the total time delay $T_0 + T_1$ no longer gives rise to a predictable trend in behavior as is found in the flux transport-dominated case and illustrated in Figure 6. In this regime, the mean amplitude of the solution remains constant with increasing $T_0 + T_1$; however, the duration of minima and the number of cycles between each minimum varies irregularly with increasing $T_0 + T_1$.

Next, looking at solutions for positive dynamo number, $N_D > 0$, we find that the form of the initial solution specified becomes important in determining the nature of the solution obtained. For initial solutions whose sign varies on a timescale comparable to or less than the diffusive timescale, it is possible to obtain solutions that are qualitatively similar to those for which $N_D < 0$. An example is shown in Figure 11, where the initial solution $A(t) = B_\phi(t) = \cos(t)$ for $t \in [-T_0 - T_1, 0]$ has been specified. This may be compared to Figure 8, where $N_D < 0$. On increasing N_D , the maximum field strength is again seen to increase, with periods of reduced activity occurring at higher dynamo numbers.

A second type of solution occurs for $N_D > 0$, in which single-signed oscillations of irregular amplitude and period are present. These solutions arise when the initial solutions vary only slowly when compared to the diffusive timescales. An example is shown in Figure 12, where the constant initial solution $A(t) = B_\phi(t) = 5$ for $t \in [-T_0 - T_1, 0]$ has been taken but the same parameters for Figure 11 are used. In these low dynamo number solutions, the minimum in magnetic energy is nonzero for sustained periods of time. On increasing the dynamo number, periods of reduced activity in these single-signed oscillations become apparent, in which the field strength is near zero between bursts of activity.

The analogy with a damped driven oscillator that is given by equation (4) can help explain some of these features. In the case in

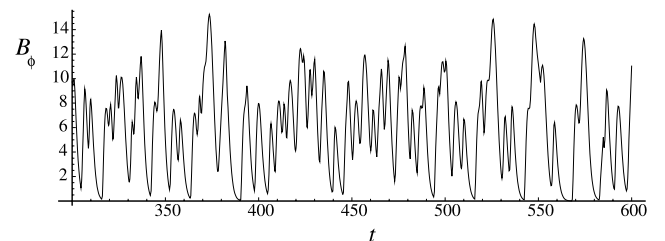


FIG. 12.—Time series for the toroidal field with $N_D > 0$ and constant initial solution. The parameters $\omega/L = -3$, $\alpha_0 = -1$, $\tau = 1$, $T_0 = 10$, and $T_1 = 4$ have been taken.

which $N_D < 0$, equations (7) and (6) may again be used to explain the point of bifurcation from a steady state to cyclic behavior. Substituting $\tau = 1$ and $T_d = 14$ into equation (7) implies that $\Omega = 0.196$ at this bifurcation, corresponding to a period of $P = 31.95$. Substituting this value for Ω into equation (6) gives the dynamo number at the point of bifurcation as $N_D = -1.039$, corresponding closely to that found in the simulations.

For a sufficiently low dynamo number the amplitude of the solution is small, and so B_ϕ is, for most of the time, within the range $[-B_{\max}, B_{\max}]$ over which the driving term on the right-hand side of equation (4) operates. When the solution is outside of this range, the high diffusivity ensures that the field decays to within this range once again on a timescale shorter than the sum of the time delays. This rapidity, when compared to the time delays, distinguishes the solution from the flux transport-dominated case, since each time the delayed solution $B_\phi(t - T_0 - T_1)$ decays to $\pm B_{\max}$, the solution $B_\phi(t)$ will have different magnitude, and may be of different sign, thus changing the nature of the driving force. In this manner the short diffusive timescales ensure that it is possible to obtain double-signed oscillations when $N_D > 0$ (which cannot be achieved in the flux transport-dominated regime). Such a solution relies on the sign of $B_\phi(t)$ being different from that of $B_\phi(t - T_0 - T_1)$ when $B_\phi(t - T_0 - T_1)$ decays to lie within the range $[-B_{\max}, B_{\max}]$. This ensures that the term on the right-hand side of equation (4), $NB_\phi(t - T_0 - T_1)$, acts to drive the solution toward a different sign. At some $t > 0$ the solution $B_\phi(t)$ will leave the range $[-B_{\max}, B_{\max}]$, but now the rapid decay of the solution has the result that $B_\phi(t - T_0 - T_1)$ may be of different sign to $B_\phi(t)$, given suitable initial conditions. Such conditions were specified in Figure 11, where double-signed oscillations occur.

4. DISCUSSION

A number of generalizations can be made to the above analysis. It has been assumed that during the flux transport no dissipative effects act on the fields: the source terms in equations (2) and (3) are proportional to ω/L and α_0 , respectively. In the most general case, the fields may be subject to dissipative losses during their transportation from one source region to another. Accordingly, extra loss factors can be introduced to the equations to take dissipation into account, which we would expect to become important only when flux transport is by spatial diffusion, specifically in the diffusion-dominated regime. In this case the general form of the equations should be

$$\frac{dB_\phi(t)}{dt} = \frac{\omega}{L} e^{-T_0/\tau} A(t - T_0) - \frac{B_\phi(t)}{\tau}, \quad (8)$$

$$\frac{dA(t)}{dt} = \alpha_0 f \left(B_\phi(t - T_1) e^{-T_1/\tau} \right) e^{-T_1/\tau} B_\phi(t - T_1) - \frac{A(t)}{\tau}. \quad (9)$$

The additional multiplicative exponential factors are close to unity (and hence unimportant) in the flux transport-dominated case, but small (and hence important) in the diffusion-dominated case. However, in both situations qualitatively similar behavior to that described in § 3 may be obtained, given a suitable rescaling of the parameters ω/L and α_0 (corresponding to an increase in dynamo number). The resultant solutions are then of greater amplitude compared with the system of equations (2) and (3), since it can be seen from equation (4) that an exponential term within the quenching factor f will have the effect of increasing the range of B_ϕ over which forcing operates.

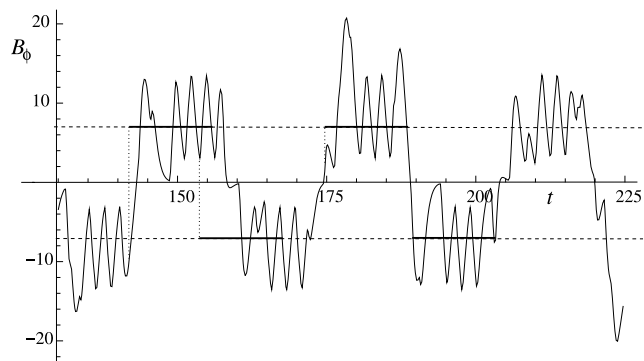


FIG. 13.—Time series for the toroidal field in the diffusion-dominated case with $N_D < 0$, using the parameters $\omega/L = -6$, $\alpha_0 = 3$, $\tau = 0.5$, $T_0 = 10$, and $T_1 = 4$. The dashed lines indicate the boundaries of the forcing region, and the thick solid lines are of length $T_0 + T_1 = 14$, corresponding to the total time delay. The first two bars have been placed to illustrate a negative sign combination of $B_\phi(t)B_\phi(t - T_0 - T_1)$ that leads to further oscillation within a half cycle, and the final two bars have been placed to illustrate the positive sign combination of $B_\phi(t)B_\phi(t - T_0 - T_1)$ present at the end of each half-cycle.

We considered a particular choice of algebraic α -effect that gives rise to the possibility of having both a lower and an upper cutoff in the range over which the α -effect operates. In the examples illustrated above, the value of B_{\min} is such that the α -effect is nonzero throughout the range $[-B_{\max}, B_{\max}]$, although its value decreases rapidly outside the range $[|B_{\min}|, |B_{\max}|]$. With an increase of B_{\min} such that there is some finite range between $[-B_{\max}, B_{\max}]$, centered at $B_\phi = 0$, where the α -effect is zero, the majority of the solution types described above can be recovered. The exceptions are the behavior at low dynamo numbers, both in the diffusion-dominated case shown in Figure 8 and in the flux transport-dominated case shown in Figure 3. These solutions rely on the quenching factor f being nonzero within $[-B_{\max}, B_{\max}]$ and on $B_\phi(t)$ being contained within that range. This is no longer the case with a higher value of B_{\min} .

We may also consider the dynamics that may be obtained in the model when the nonlinear term, f , which parameterizes α -quenching is set to be a constant, $f = 1$, say, thus making the system linear. Simple linear models of interface dynamos have previously been considered, in which communication between the two source layers takes place by diffusion alone (see, for example, Moffatt 1978, p. 216; MacGregor & Charbonneau 1997). In the time-delay model presented here, a variety of solutions may be obtained when $f = 1$, all of which are present independent of the relative magnitudes of τ , T_0 , and T_1 . When the magnitude of the dynamo number, $|N_D|$, is low, decaying solutions result. For sufficiently high $|N_D|$, growing solutions are obtained. The transition state between these two regimes is dependent on the sign of N_D . For $N_D < 0$ cyclic solutions are obtained, which are qualitatively similar to those illustrated in Figure 3. For $N_D > 0$, steady state solutions are obtained in which the magnetic fields are nonzero, but do not change in time.

If an explanation of both the flux transport-dominated and diffusion-dominated regimes in terms of an analogy with a damped driven oscillator can be invoked, then the nature of the driving term (given by the right-hand side of eq. [4]) is important. In the first case, since the diffusive timescales are long when compared to the time delays, once the solution $B_\phi(t)$ is not within the range $[-B_{\max}, B_{\max}]$ for all time, the sign combination $B_\phi(t)B_\phi(t - T_0 - T_1)$ will always be positive when the driving term begins to act during the declining phase of each cycle. This predictability leads to the regularity in the system, to the single-signed oscillations for $N_D > 0$, and to the double-signed oscillations

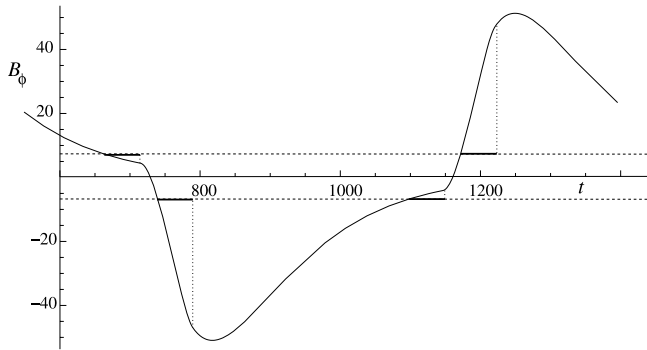


FIG. 14.—Time series for the toroidal field in the flux transport–dominated case with $N_D < 0$, using the parameters $\omega/L = -0.008$, $\alpha_0 = 0.008$, $\tau = 100$, $T_0 = 40$, and $T_1 = 10$. The dashed lines indicate the boundaries of the forcing region, and the thick solid lines are of length $T_0 + T_1 = 50$, corresponding to the total time delay. The bars have been placed to illustrate first the change in the gradient of the solution as $B_\phi(t - T_0 - T_1)$ enters the forcing region (before which the solution is purely diffusive) and second the switch in the solution from being driven to being purely diffusive as the solution $B_\phi(t - T_0 - T_1)$ leaves the forcing region.

for $N_D < 0$. In the second case, since the rapid diffusivities ensure that the solution returns to the forcing region in a timescale shorter than the time delays, the sign combination $B_\phi(t)B_\phi(t - T_0 - T_1)$ will not be fixed as in the diffusive case. Thus, the sign of the driving term will vary between cycles and within each half-cycle, leading to irregularity in the system. Figures 13 and 14 illustrate these effects. They show typical solutions in each of the regimes, with bars corresponding to the length of the time delays superimposed on the solution to illustrate the sign combinations of $B_\phi(t)B_\phi(t - T_0 - T_1)$ and, in the flux transport–dominated case, the change in the gradient of the solution as it enters the forcing region.

5. CONCLUSIONS

To summarize, we have constructed a physically motivated reduced stellar dynamo model, which includes time delays (in the flux transport), to study the effects of spatial segregation of the dynamo source regions in stellar convection zones. The model can be generalized to study a diverse set of α -effect mechanisms located at different layers in stellar convection zones, such as the tachocline, or the base of the convection zone, or near the surface. This can be achieved by varying the time delays to appropriately account for the dominant flux transport mechanisms that are unique to a specific dynamo model based on a particular α -effect mechanism. This can be, for example, the meridional circulation timescale in Babcock-Leighton dynamo models, or the turbulent pumping timescale in interface (or other) dynamo models that do not rely on meridional circulation. Motivated by stellar activity observations and the wide parameter space they offer, we have explored the dynamics of our model by increasing the dynamo number N_D (consequently reducing the Rossby number Ro), specifically for two extreme regimes.

In the flux transport–dominated regime, some similarity to the solar cycle is seen. On increasing the dynamo number, a transition from no magnetic activity to oscillatory behavior occurs. The solutions show polarity reversal, however, only in the case of negative dynamo number, which, when the differential rotation ω/L is assumed to be negative (as is observed in the high-latitude part of the solar tachocline), corresponds to a positive α -effect (as is the case in the Babcock-Leighton mechanism). The steep rising phase and longer declining phase resemble those of the sunspot cycle; the similarity of the solar cycle to a nonlinear

relaxation oscillator was noted in Mininni et al. (2001). As expected, on increasing the dynamo number, the level of magnetic activity increases. Although the period of the magnetic cycle is significantly longer than both the length of the time delays and the diffusive timescales, the expected qualitative behavior of the dynamo (i.e., increasing period of oscillation and amplitude with increasing time delays) is recovered. However, events such as grand minima would be hard to explain in this model regime without invoking some form of stochasticity in the poloidal source term or including some other physics. Nevertheless, given the similarity of the solutions in this case with other aspects of the solar cycle, we conclude that the solar dynamo is possibly (in its present state of activity) in the flux transport–dominated regime.

The model is capable of irregular behavior, including significant amplitude modulation, in the diffusion-dominated regime. In this case the magnetic cycle shows polarity reversal for both positive and negative dynamo numbers and has an average length, about which it shows small variations. The average length of each magnetic cycle is on the same order as the sum of the two time delays. Amplitude modulation is seen for solutions along a cut through parameter space corresponding to increasing dynamo numbers, although the character of the modulation varies considerably. For small dynamo numbers, episodes of minimal activity are present that are short compared to the cycle period and that are spaced irregularly in time. On increasing the dynamo number, the duration of events becomes longer and is regular in both length and spacing for larger dynamo numbers. These phases of reduced activity are reminiscent of the solar Maunder minima; however, the overall nature of the magnetic activity is qualitatively similar to many stars in the Mount Wilson project that show highly irregular behavior. This may imply that these latter stars, which exhibit irregular magnetic activity, support dynamos whose underlying physics is similar to the diffusion-dominated regime of our model.

It would be possible to take a cut through parameter space, corresponding to increasing dynamo number, that links both of these regimes. Taking an increase in $|\alpha_0\omega/L|$ but a decrease in τ in such a way as to increase $|N_D|$ moves solutions from the regular oscillations present in the flux transport–dominated regime to the irregular nature of the diffusion-dominated regime and increases the level of magnetic activity. This is exactly the behavior observed in solar-like stars, whose magnetic activity is distinguished by rotation rate (recall that a low Rossby number Ro corresponds to a high dynamo number N_D). While this particular cut through parameter space may be artificial because it is not clear how field diffusivities are affected by rotation rate, the principle of increasing a system parameter and observing a qualitative change in solutions provides an useful analogy to stellar activity observations (Saar & Brandenburg 1999).

Our studies have implications for understanding the long-term evolution of the solar dynamo mechanism. Deciphering solar variability over very long (up to stellar and planetary evolutionary) timescales is relevant for space climate studies that seek to understand the impact of solar forcing on the evolution and formation of planetary systems and on the electromagnetic environment within the heliosphere (see Nandy & Martens 2006 for detailed discussions on how studies such as these fit into the larger context of the space climate). Specifically, the dynamo activity of a star such as the Sun evolves over the lifetime of the star with the evolution of the properties of its convection zone. In particular, the rotation rate decreases because of angular momentum losses via stellar winds. This results in an increase in the value of the Rossby number (Ro) and a corresponding decrease in the dynamo number (N_D) with time. As is evident from our study, varying the dynamo

number results in solutions with different cycle amplitudes (with the expected positive correlation), and indeed, in some extreme cases, results in magnetic activity with a completely different behavior. Therefore, through studies such as this, in which exploration of a wide range of dynamo parameter space is possible, one can implicitly derive conclusions about the long-term evolution and behavior of the dynamo mechanism in a solar-like star.

In conclusion, we note that time delays in the dynamo equations are capable of producing a wide range of activity in stellar dynamos, including regular cycles, period-amplitude modulation, and episodes of reduced activity. This clearly demonstrates the

importance of flux transport time delays in models of solar and stellar dynamos.

We thank an anonymous referee for useful discussions. Studies of solar and stellar dynamos at Montana State University are supported by a NASA Living With a Star grant NNG05GE47G. We also acknowledge support from the UK PPARC and the Montana State University Solar Physics Research Experience for Undergraduates Program. G. H. and A. L. W.-S. wish to thank the MSU Solar Physics group for their hospitality and financial support.

REFERENCES

- Babcock, H. W. 1961, *ApJ*, 133, 572
- Baliunas, S. L., Donahue, R. A., Soon, W., & Henry, G. W. 1998, in ASP Conf. Ser. 154, *The Tenth Cambridge Workshop on Cool Stars, Stellar Systems and the Sun*, ed. R. A. Donahue & J. A. Bookbinder (San Francisco: ASP), 153
- Baliunas, S. L., et al. 1995, *ApJ*, 438, 269
- Beer, J., Blinov, A., Bonani, G., Hofmann, H. J., & Finkel, R. C. 1990, *Nature*, 347, 164
- Beer, J., Tobias, S. M., & Weiss, N. O. 1998, *Sol. Phys.*, 181, 237
- Charbonneau, P. 2001, *Sol. Phys.*, 199, 385
- . 2005, *Living Rev. Sol. Phys.*, 2, 2
- Charbonneau, P., St-Jean, C., & Zacharias, P. 2005, *ApJ*, 619, 613
- Chatterjee, P., Nandy, D., & Choudhuri, A. R. 2004, *A&A*, 427, 1019
- Covas, E., & Tavakol, R. 1997, *Phys. Rev. E*, 55, 6641
- Dikpati, M., & Charbonneau, P. 1999, *ApJ*, 518, 508
- Dikpati, M., & Gilman, P. A. 2001, *ApJ*, 559, 428
- D'Silva, S., & Choudhuri, A. R. 1993, *A&A*, 272, 621
- Durney, B. R. 1997, *ApJ*, 486, 1065
- . 2000, *Sol. Phys.*, 196, 421
- Durney, B. R., & Latour, J. 1978, *Geophys. Astrophys. Fluid Dyn.*, 9, 241
- Eddy, J. A. 1988, in *Secular Solar and Geomagnetic Variations in the Last 10,000 Years*, ed. F. R. Stephenson & A. W. Wolfendale (NATO ASI Ser. C, 236; Dordrecht: Kluwer), 1
- Fan, Y., Fisher, G. H., & McClymont, A. N. 1994, *ApJ*, 436, 907
- Ferriz-Mas, A., Schmitt, D., & Schüssler, M. 1994, *A&A*, 289, 949
- Hathaway, D. H., Nandy, D., Wilson, R. M., & Reichmann, E. J. 2003, *ApJ*, 589, 665
- Hempelmann, A., Schmitt, J. H. M. M., & Stepień, K. 1996, *A&A*, 305, 284
- Leighton, R. B. 1969, *ApJ*, 156, 1
- MacGregor, K. B., & Charbonneau, P. 1997, *ApJ*, 486, 484
- Mininni, P. O., Gomez, D. O., & Mindlin, G. B. 2001, *Sol. Phys.*, 201, 203
- Moffatt, H. K. 1978, *Magnetic Field Generation in Electrically Conducting Fluids* (Cambridge: Cambridge Univ. Press)
- Montesinos, B., Thomas, J. H., Ventura, P., & Mazzitelli, I. 2001, *MNRAS*, 326, 877
- Nandy, D. 2002, *Ap&SS*, 282, 209
- . 2003, in *Proceedings of SOHO 12/GONG+ 2002, Local and Global Helioseismology: The Present and Future*, ed. H. Sawaya-Lacoste (ESA SP-517; Noordwijk: ESA), 123
- . 2004a, *Sol. Phys.*, 224, 161
- . 2004b, in *Proceedings of SOHO 14/GONG 2004, Helio- and Astero-seismology: Towards a Golden Future*, ed. D. Danesy (ESA SP-599), 241
- Nandy, D., & Choudhuri, A. R. 2002, *Science*, 296, 1671
- Nandy, D., & Martens, P. C. H. 2006, in *Proceedings of the International Living With a Star Workshop 2006 (Goa, India)*, ed. N. Gopalswamy, in press
- Noyes, R. W., Hartmann, L. W., Baliunas, S. L., Duncan, D. K., & Vaughan, A. H. 1984a, *ApJ*, 279, 763
- Noyes, R. W., Weiss, N. O., & Vaughan, A. H. 1984b, *ApJ*, 287, 769
- Ossendrijver, M. 2003, *A&A Rev.*, 11, 287
- Parker, E. N. 1955, *ApJ*, 122, 293
- . 1993, *ApJ*, 408, 707
- Roald, C. B., & Thomas, J. H. 1997, *MNRAS*, 288, 551
- Saar, S. H., & Brandenburg, A. 1999, *ApJ*, 524, 295
- Schmalz, S., & Stix, M. 1991, *A&A*, 245, 654
- Schou, J., et al. 1998, *ApJ*, 505, 390
- Tobias, S. M. 1997, *A&A*, 322, 1007
- Tobias, S. M., Brummell, N. H., Clune, T. L., & Toomre, J. 2001, *ApJ*, 549, 1183
- Tobias, S. M., Weiss, N. O., & Kirk, V. 1995, *MNRAS*, 273, 1150
- Weiss, N. O., Cattaneo, F., & Jones, C. A. 1984, *Geophys. Astrophys. Fluid Dyn.*, 30, 305
- Wilmot-Smith, A. L., Martens, P. C. H., Nandy, D., Priest, E. R., & Tobias, S. M. 2005, *MNRAS*, 363, 1167
- Yoshimura, H. 1978, *ApJ*, 226, 706